Communication

Direct Cold Sintering of α-Al_2O_3 Ceramics in a Pure Water Medium

Anastasia A. Kholodkova *, Maxim V. Kornyushin, Arseniy N. Khrustalev, Levko A. Arbanas, Andrey V. Smirnov, Yurii D. Ivakin

Posted Date: 7 May 2024

doi: 10.20944/preprints202405.0366.v1

Keywords: gibbsite; boehmite; alumina; cold sintering process; porous ceramics

Communication

Direct Cold Sintering of α-Al_2O_3 Ceramics in a Pure Water Medium

Anastasia A. Kholodkova [1,*], Maxim V. Kornyushin [1], Arseniy N. Khrustalev [2], Levko A. Arbanas [2], Andrey V. Smirnov [2] and Yurii D. Ivakin [3,4]

[1] Statistics Department, Department of Scientific Research Coordination, State University of Management, 109545 Moscow, Russia; maksim.korn0312@yandex.ru (M.V.K.)
[2] Laboratory of Ceramic Materials and Technology, MIREA - Russian Technological University, 119454 Moscow, Russia; lywn@yandex.ru (A.N.K.); levko.147@icloud.com (L.A.A.); smirnov_av@mirea.ru (A.V.S.)
[3] Mobile Solutions Engineering Center, MIREA - Russian Technological University, 119454 Moscow, Russia; ivakin@kge.msu.ru (Y.D.I.)
[4] Chemistry Department, Lomonosov Moscow State University, 119991 Moscow, Russia; ivakin@kge.msu.ru (Y.D.I.)
* Correspondence: anastasia.kholodkova@gmail.com

Abstract: Porous α-Al_2O_3 ceramics is a highly demanded material for multitude applications such as filters, substrates, biomedicine materials, etc. Despite the availability of the raw materials, a challenge of their technology is in a high energy budget caused by the sintering above 1500 °C. For a cold sintering processing (CSP) of ceramics, the lowering of α-Al_2O_3 sintering temperature is one of the most urgent challenges at the background of its rapid development. The current paper for the first time demonstrates the solution of the mentioned problem by the CSP of α-alumina ceramics in a presence of pure water as a transient liquid. The manufactured materials were examined by XRD analysis; the evolution of their microstructures during the CSP was revealed by SEM, and the porosity evaluated by the Archimedes method. The ceramics with an open porosity up to 36 % was produced at 380-450 °C, 220 MPa in 30 min. An increase in the pressure was found to impede α-Al_2O_3 formation from γ-AlOOH. The development of the microstructure was discussed within the frameworks of the dissolution-precipitation model and the homogenous nucleation. The results of the SEM study pointed to the coalescence of γ-AlOOH grains during the CSP.

Keywords: gibbsite; boehmite; alumina; cold sintering process; porous ceramics

1. Introduction

Cold sintering process (CSP) introduced by Randall et al. in 2016 [1] is known as a rapidly developing technique for an express and energy-saving production of ceramic and composite materials, the range of which is expanding annually. Providing materials consolidation and sintering at a tremendously lowered temperature, the CSP was applied to the ceramics and composites manufacturing as an alternative to the high-temperature as well as multistage techniques. The processes accompanying the CSP are commonly interpreted by the dissolution-precipitation mechanism [2]. At the initial stage, the transient liquid acts similar to the temporary technological binder in the uniaxial compaction of powders facilitating the particles rearrangement. Next, on heating, it might partially dissolve the solid particles and transport the substance from the high- to low-stress surface regions. For the moment, materials with more than a hundred compositions have been densified using the CSP including those which are unavailable for the traditional routes because of their thermodynamic incompatibility [3–7].

An upgrade in an energy budget embedded in CSP is highly desirable to produce materials with extremely high sintering temperature, for example, refractories. Several authors reported a success in manufacturing of electrolyte materials such as those based on yttria-stabilized zirconia [8–10] and sodium-β-alumina [11], also magnesia ceramics [12] *via* single CSP or combined with post heat treatment (PHT) 1200-1300 °C. Conventionally sintered above 1400 °C, these oxides were densified

 doi:10.20944/preprints202405.0366.v1

up to 83-93% of their theoretical density and preserved a fine-grained microstructure due to CSP at temperatures of about 30% of their melting points. However, such examples remain far from numerous against the background of achievements in CSP.

The most stable α-modification of alumina (α-Al_2O_3) is a well-known refractory material (sintered above 1500 °C) with a wide application range from abrasion to microelectronic and biomedical materials. α-Al_2O_3 is highly appreciated due to a combination of chemical stability, mechanical strength, dielectric properties, biological compatibility, and availability [13–15]. In particular, porous α-Al_2O_3 ceramics are of interest for liquid and gas filters, supports for catalysts and metal-organic frameworks (MOFs) [16–19]. Ohji et al. [20] in their review classified the approaches for preparation of a macroporous ceramic structures in four categories: partial sintering, the use of a sacrificial templates, replica technique, and direct foaming. In recent years, the alumina porous ceramics was reported to be manufactured following the methods mentioned above [21–24] as well as *via* a rapidly developing 3D printing techniques [25,26] with a precise control of its pore structure. However, these approaches always conceal a compromise of the achieved properties on one hand and a multi-stage, energy consumption, high-cost auxiliary compounds and equipment on another.

For the moment, several works demonstrated an application of the CSP to manufacture alumina ceramics. Herisson de Beauvoir et al. [27] prepared semi-transparent material consisting of boehmite and amorphous alumina by processing of aluminum hydroxide hydrate at temperatures up to 400 °C and a pressure of 500 MPa for 30-180 min. PHT at 500 °C in air led to a formation of γ-Al_2O_3. Kang et al. [28] performed CSP of mixed γ- and α-Al_2O_3 in a medium of glacial acetic acid at 300 °C and 300 MPa for 1 h. The PHT above 1250 °C led to highly dense α-Al_2O_3 ceramics. Suleiman et al. [29] applied CSP for the compaction of Al_2O_3-NaCl composites which transformed into porous alumina ceramics on PHT at 1200-1500 °C for 30 min. Later, Gao et al. [30] demonstrated a direct preparation of γ-Al_2O_3 translucent ceramics by the CSP in 10 M NaOH at 350 °C and 500 MPa without a need of PHT.

Our previous work [31] showed a capability of CSP combined with spark plasma sintering (SPS) to obtain porous boehmite material which transformed in α-Al_2O_3 ceramics with a porosity of about 60 % on the PHT. In this case, γ-$Al(OH)_3$ was used as a raw powder. Besides, a formation of α-Al_2O_3 in CSP-SPS conditions was observed at 450 °C and 70 MPa in a presence of 5 wt.% of water, but the material demonstrated a poor transport strength. In the current research, we develop the CSP for a direct obtaining of a porous α-Al_2O_3 ceramics starting from γ-$Al(OH)_3$ powder following the previous results. The work reveals the effects of the processing temperature and pressure on the phase and microstructural transformations during the CSP of alumina in a presence of pure water.

2. Materials and Methods

Gibbsite γ-$Al(OH)_3$ (> 99.6 % purity, Pikalevo Alumina Refinery LLC, Pikalevo, Russia) and α-Al_2O_3 (Treibacher Industrie AG, Althofen, Austria) powders were used as starting materials in the CSP. The characterization of the initial powders by X-ray diffraction (XRD) and scanning electron microscopy (SEM) is presented in Appendix A (Figures A1, A2). A mixture of 95 wt. % γ-$Al(OH)_3$ and 5 wt. % α-Al_2O_3 was prepared by a quintuple joint sieving through a sieve with a 300 μm cell. The role of α-Al_2O_3 additive was to promote alumina nucleation during the cold sintering. Earlier, such effect of α-Al_2O_3 seeding was reported for the synthesis of its fine crystals in supercritical water [32] as well as for the conventional sintering from aluminum hydroxide at a lowered temperature [33]. The prepared mixture (1.000 g) was placed inside a mold equipped with a circular heater and a thermal insulation cover. Then, 0.2 ml of distilled water were added to the powder inside of the mold. Graphite sheets separated the inner wall of the mold and the punches from the prepared suspension. The filled mold was placed between the platforms of a uniaxial press, and a pressure of 90-350 MPa was applied to it. Then, the mold was heated up to a temperature of 380-450 °C with a rate of 860 °C h^{-1} and held isothermally under the applied pressure for 30 min. After that, the pressure was relieved, and the mold cooled down to the room temperature. The obtained ceramic sample was removed from the mold and peeled from the graphite sheets.

 doi:10.20944/preprints202405.0366.v1

The phase compositions of the initial powders and the obtained ceramic samples were studied by XRD method using Rigaku D/Max-2500 diffractometer (Rigaku Corp., Tokyo, Japan). Identification of the phases was provided with the use of PDF2 database [34]. Diffraction pattern profile fitting was carried out following the Le Bail method by the means of FullProf software [35]. The initial structural models were taken from the Crystallography Open Database [36]. The Rietveld method [37] was applied for the quantitative phase analysis of the ceramic samples. Microstructural study of the powders and ceramics was provided at Jeol JSM 6380 scanning electron microscope (Jeol Ltd., Tokyo, Japan). Particle and grain size distributions based on the measurements in the SEM images carried out using ImageJ software [38]. The density and porosity measurements were carried out following the Archimedes method with the use of kerosene as a saturating liquid.

3. Results

Cold sintering of the gibbsite powder mixed with 5 wt. % of α-alumina in a presence of 20 wt. % of distilled water as a transient liquid resulted in a formation of solid and transportable ceramic samples, an example of which is shown in Figure 1.

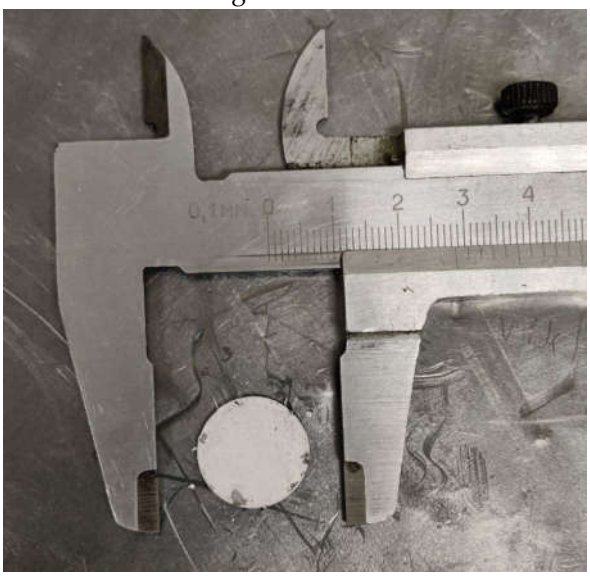

Figure 1. Alumina ceramics manufactured by the CSP with an addition of 20 wt. % of distilled water (processing parameters: 450 °C, 220 MPa).

A mechanical pressure initially applied to the mold containing the starting powder mixture and an amount of distilled water significantly affected the phase contents of the final ceramic samples. Figure 2a shows the XRD patterns of the samples obtained by CSP at 450 °C under different values of the mechanical pressure. At the lowest pressure of 90 MPa, γ-$Al(OH)_3$ powder transformed into a mixture of α-Al_2O_3 (51.6 wt. %), χ-Al_2O_3, and a small amount of boehmite (γ-AlOOH) (Figure 2b). The increase in the pressure up to 220 MPa resulted in a complete transformation of γ-$Al(OH)_3$ into α-alumina. However, the further rise of the mechanical pressure to 350 MPa led to a formation of ceramics which consisted of 81.6 wt.% γ-AlOOH and only 18.4 wt.% of α-Al_2O_3 (Figure 2b). Carbon and silica impurities detected in XRD pattern got into the sample prepared at 220 MPa from the graphite paper, which contacted with the sample during the CSP, and a mortar used for the ceramics grinding before the XRD analysis.

 doi:10.20944/preprints202405.0366.v1

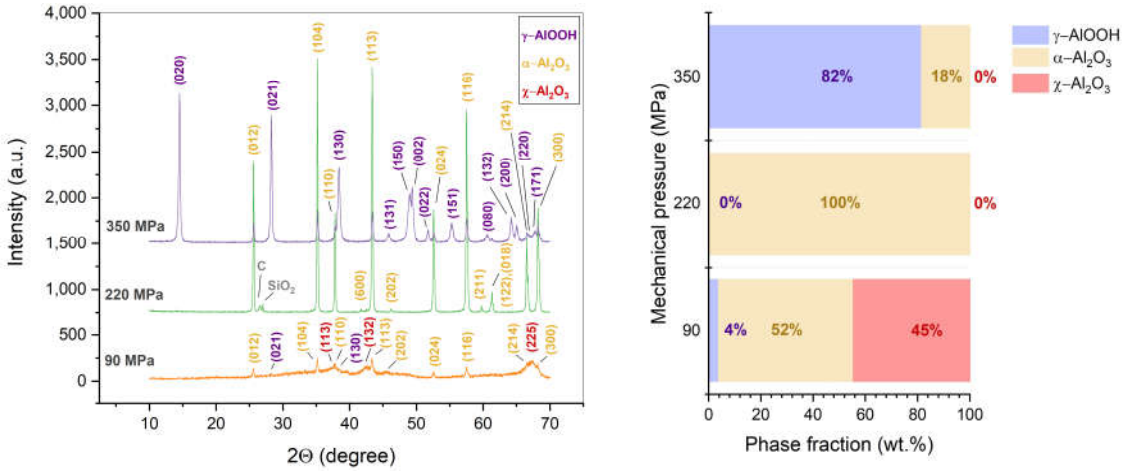

(**a**) (**b**)

Figure 2. XRD patterns (**a**) and phase fractions (**b**) of the ceramic samples manufactured by CSP at 450 °C and indicated mechanical pressure (90-350 MPa). Miller indices correspond to the following phases: γ-AlOOH (PDF2 #000-83-2384), α-Al_2O_3 (PDF2 #000-71-1683), and χ-Al_2O_3 (PDF2 #000-04-0880). Phase fractions are presented excluding foreign impurities.

The effect of CSP temperature on the phase contents of the alumina ceramics at a constant mechanical pressure is shown in Figure 3. A major phase of α-Al_2O_3 was found in the samples obtained at 380-450 °C and a pressure of 220 MPa. However, the ceramics manufactured at 410 °C contained a minor phase of boehmite (γ-AlOOH) in an amount of 5.1 wt.%. A metal (Fe) admixture is supposed to be brought into the sample from the inner surfaces of the mold.

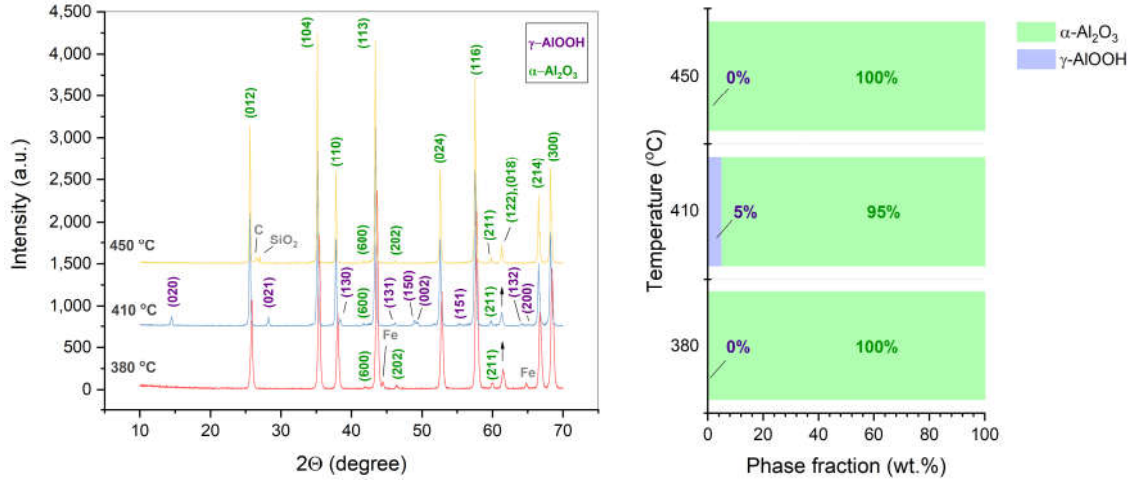

(**a**) (**b**)

Figure 3. XRD patterns (**a**) and phase fractions (**b**) of the ceramic samples manufactured by CSP at a pressure of 220 MPa and indicated temperature (380-450 °C). Miller indices correspond to the following phases: γ-AlOOH (PDF2 #000-83-2384) and α-Al_2O_3 (PDF2 #000-71-1683). Phase fractions are presented excluding foreign impurities.

At a mechanical pressure of 350 MPa, the samples formed in a temperature range of 380-450 °C contain a major part of boehmite (Figure 4a). The rise of the CSP temperature resulted in an increase in α-Al_2O_3 fraction in these samples from 4.9 to 18.4 wt.% (Figure 4b).

 doi:10.20944/preprints202405.0366.v1

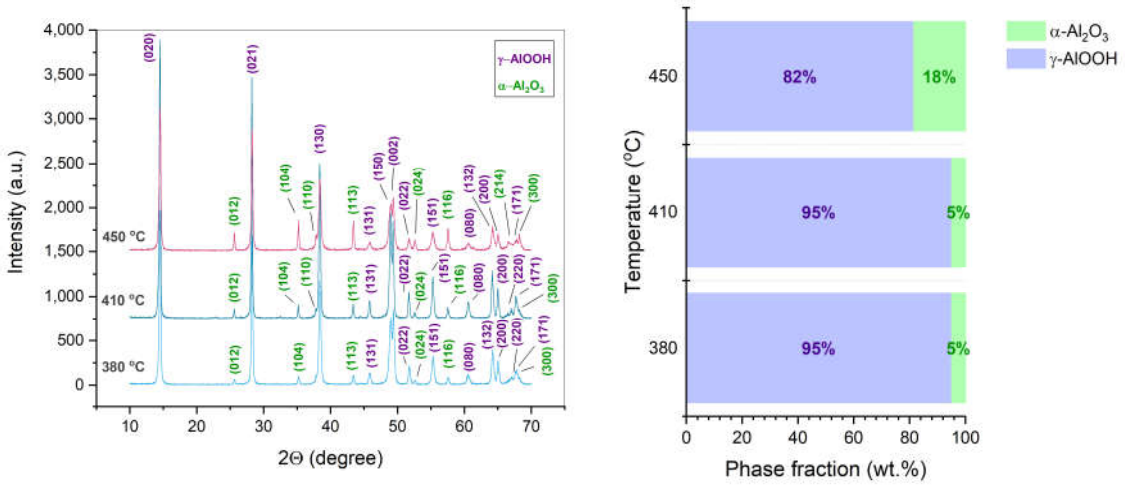

(**a**) (**b**)

Figure 4. XRD patterns (**a**) and phase fractions (**b**) of the ceramic samples manufactured by CSP at a pressure of 350 MPa and indicated temperature (380-450 °C). Miller indices correspond to the following phases: γ-AlOOH (PDF2 #000-83-2384) and α-Al_2O_3 (PDF2 #000-71-1683).

Crystallinity of boehmite and α-Al_2O_3 phases formed in CSP conditions was estimated by their mean crystallite sized calculated from XRD data (Table 1). After CSP at 220 MPa, boehmite performs slightly higher mean crystallite size (6.48 nm) than it results from the processing at 350 MPa (4.94 nm) at an equal temperature of 410 °C. γ-AlOOH to α-Al_2O_3 transformation was accompanied by a decrease in the crystallite size during the CSP at 220 MPa. On the opposite, when sintered at a pressure of 350 MPa, α-Al_2O_3 demonstrated an increase in its crystallite size compared to the neighboring boehmite phase. Crystallite sizes observed in α-Al_2O_3 were mainly higher in the case of CSP at 350 MPa than at 220 MPa. Low peak intensities in the XRD pattern of the sample obtained at 90 MPa impeded an accurate estimation of crystallite sizes of the phases it contained.

Table 1. Structural characteristics of the ceramic samples manufactured *via* CSP with 20 wt.% of water as a transient liquid.

Mechanical pressure (MPa)	Temperature (°C)	Average crystallite size (nm)		Density (g cm^{-1})	Relative density (%)	Open porosity (%)
		γ-AlOOH	α-Al_2O_3			
90	450	-	-	2.23	58.2	41.0
220	380	-	4.20	2.53	63.7	36.0
	410	6.48	5.68	2.51	64.0	35.7
	450	-	6.68	2.58	65.0	34.6
350	380	4.17	6.08	1.95	62.6	35.3
	410	4.94	7.17	1.98	63.6	28.4
	450	3.66	5.49	2.08	64.4	22.8

Relative density of the manufactured alumina ceramics calculated with respect to its phase contents did not exceed 65 % (Table 1). The values of the measured open porosity pointed to the domination of this type of the pores in the samples obtained at 90 and 220 MPa as well as in ceramics sintered at 380 °C at a pressure of 350 MPa. Lowering of the open porosity in a couple of samples processed at 410 and 450 °C with an applied pressure of 350 MPa indicates the pores' closure in these conditions. The proportion of the closed pores reached 8.0 and 12.8 % in the mentioned samples, respectively.

A large intergranular pore space in α-Al_2O_3 ceramics obtained at a pressure of 220 MPa and temperatures of 380 and 450 °C could be observed in their fractured surfaces (Figure 5), which is in accordance with the measurements of the porosity. The grains possess mostly irregular shapes and

 doi:10.20944/preprints202405.0366.v1

broad size distributions from submicron up to ten microns. The mean values of the grain size are rather close in these ceramic samples and reach about 3 μm. Locally, the grains demonstrate intergrowth and coalescence, but their major part is at the stage of neck formation between the neighboring ones.

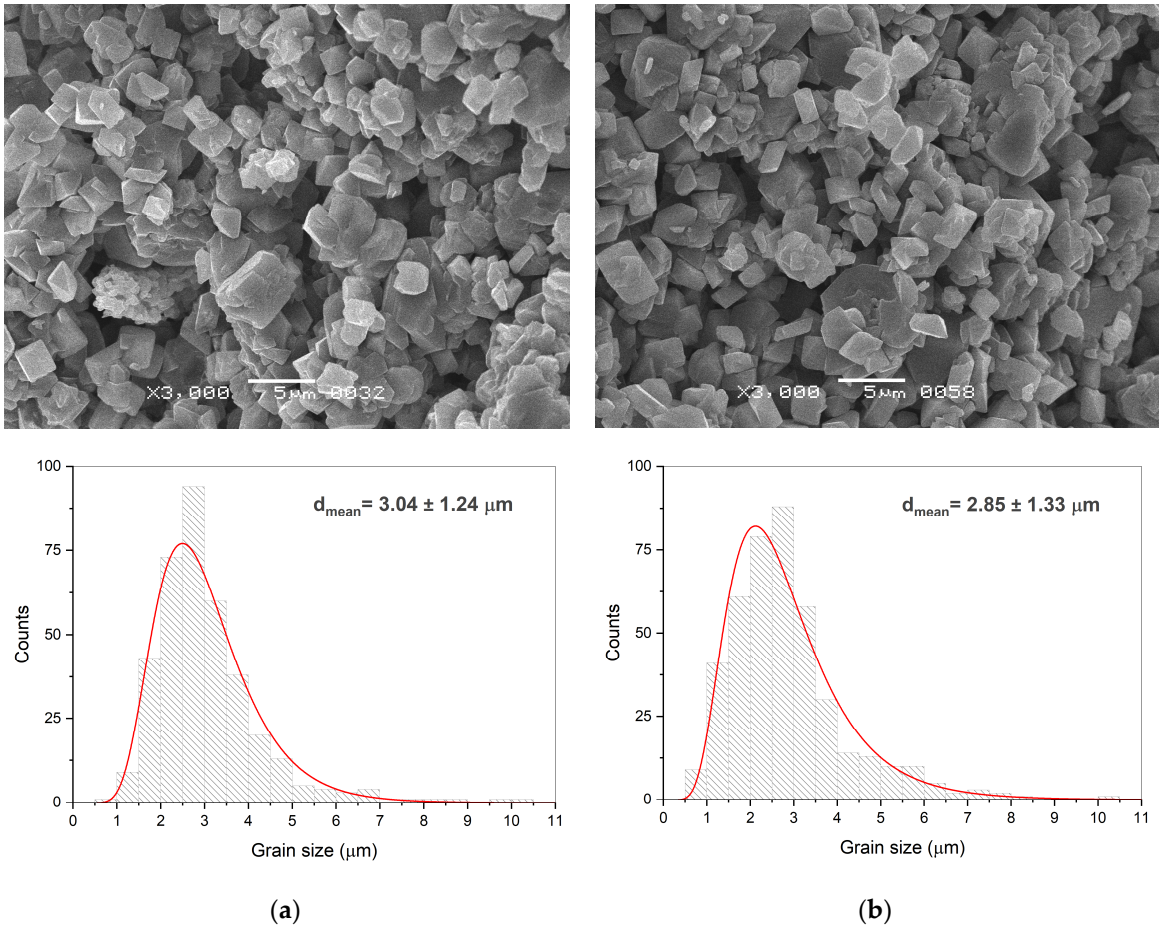

Figure 5. Fractured surfaces SEM images of the ceramics manufactured by CSP at a mechanical pressure of 220 MPa and a temperature of 380 °C (**a**) and 450 °C (**b**). Corresponding grain size distributions were calculated on the base of 400 measurements of the grain size in each of the samples.

Formed at 350 MPa and 380 °C, the boehmite ceramics consist of submicron-sized grains with a smoothed slightly elongated shape (Figure 6a). Fine-grained regions are separated by a large pore space. Noteworthy that the neighboring grains support unidirectional orientation. An increase of the CSP temperature to 410 °C led to the appearance of single plate-like grains of 2-4 μm in diameter among the fine matrix (Figure 6b). After CSP at 450 °C, the trend to the mutual orientation of the neighboring grains continues among submicron rounded as well as micron-sized plate-like ones leading to their coalescence and the formation of faceted grains (Figure 6c, d). The latter are apparently attributed to α-Al_2O_3 which phase fraction significantly increased after the CSP at 450 °C compared to the processing at lower temperatures. The size of the mentioned alumina grains was comparable to that determined for α-Al_2O_3 formed at 220 MPa (Figure 5).

 doi:10.20944/preprints202405.0366.v1

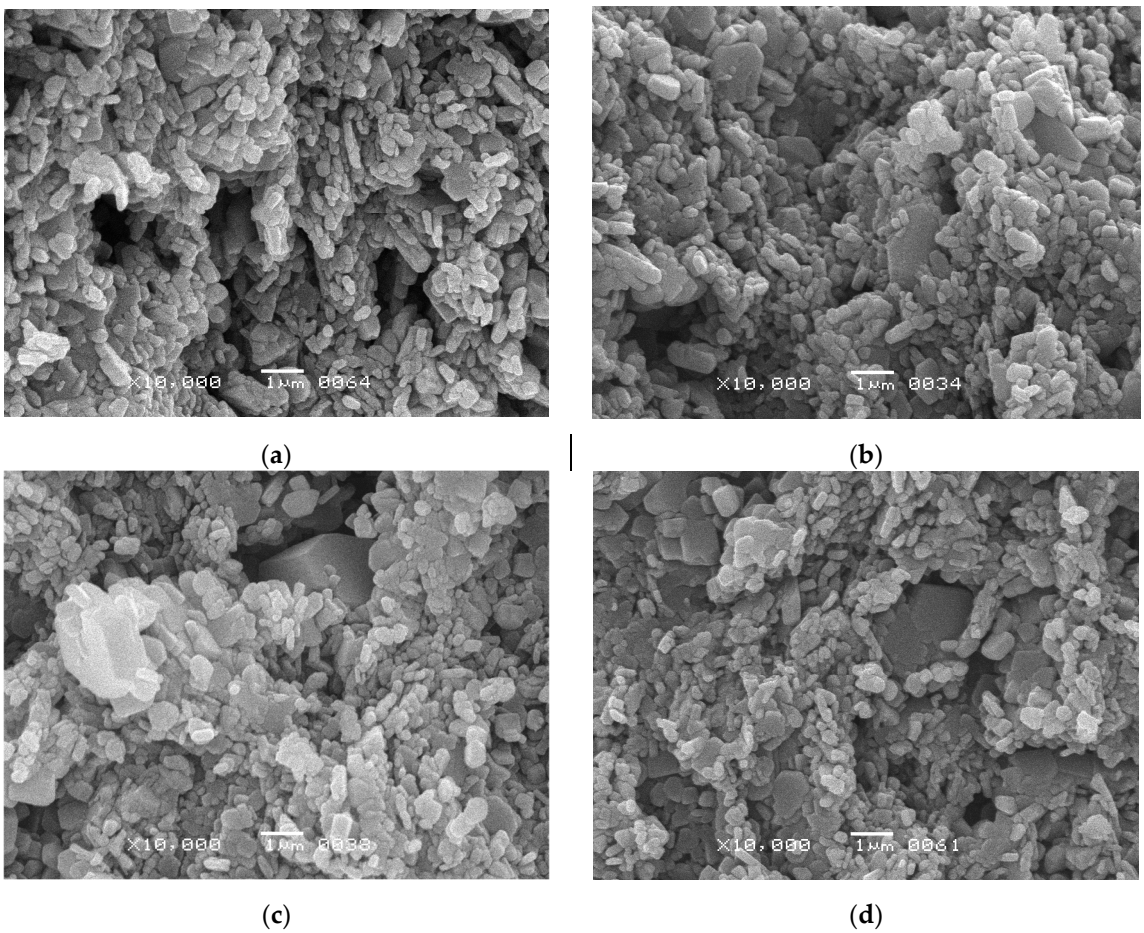

(**a**) (**b**)

(**c**) (**d**)

Figure 6. SEM images of fractured surfaces of ceramics manufactured by CSP at a mechanical pressure of 350 MPa and a temperature of 380 °C (**a**), 410 °C (**b**), and 450 °C (**c,d**).

4. Discussion

Being heated in air at about 300 °C gibbsite γ-$Al(OH)_3$ is commonly known to decompose into boehmite γ-AlOOH, which eliminates water at about 500-550 °C with the formation of γ-Al_2O_3. The latter undergoes a sequence of transformations to δ- and θ-alumina modifications and finally forms α-Al_2O_3 above 1050 °C [39,40]. In this way, the transitional phases perform face-centered cubic packing of oxygen ions. Another way from γ-$Al(OH)_3$ to α-Al_2O_3 in an air atmosphere includes the formation of χ- and κ-alumina phases with hexagonal close-packed oxygen ions above 300 °C [39]. In a water medium (below as well as above the critical point of 374 °C, 22.1 MPa), the route from gibbsite to α-Al_2O_3 was reported to pass only through the formation of boehmite, which transforms directly into α-alumina [32,41,42]. In the current work, the heating of γ-$Al(OH)_3$ powder occurred in a presence of supercritical water as the applied mechanical pressure (> 90 MPa) and the temperature of isothermal dwell (> 380 °C) exceeded the critical parameters. Under these conditions, the formation of three new phases was observed, i.e. γ-AlOOH, χ- and α-Al_2O_3. All these phases were detected in the ceramics processed at 450 °C and 90 MPa. Worth noting that the starting gibbsite placed inside the mold for the CSP, experienced a heating with a relatively high rate. Earlier, Ingram-Jones et al. [43] [https://doi.org/10.1039/JM9960600073] reported that fast heating of fine γ-$Al(OH)_3$ (0.5 μm) powder mostly resulted in a sequence of phase transitions, first of which was its transformation to χ-Al_2O_3, while the coarse gibbsite particles (14 μm) prone to form boehmite as well as χ-Al_2O_3 at the initial step of their thermal decomposition. Gibbsite powder used in the current work could be classified as a fine-grained (Figure A1), and the formation of χ-Al_2O_3 during its relatively fast heating appears expectable. Along with χ-Al_2O_3, γ-AlOOH is supposed to form from gibbsite at 90 MPa and then almost completely decompose into α-Al_2O_3. In the samples prepared at a higher mechanical pressure, χ-Al_2O_3 was not found. At 220 MPa and 450 °C, a single-phase α-alumina apparently

 doi:10.20944/preprints202405.0366.v1

formed from an intermediate boehmite phase. However, after the CSP at 350 MPa and 450 °C, α-Al_2O_3 became a minor phase in the ceramic sample mostly containing of boehmite. The mentioned observations indicated that the initial step in the CSP of gibbsite was its dehydroxylation, the route of which depended on the mechanical pressure. The rise of the applied pressure hindered the elimination of OH-groups from the solid because of the related increase in the supercritical water density inside of the mold. Almost regardless of the temperature, α-Al_2O_3 dominated in the ceramics obtained at 220 MPa, while the samples prepared at 350 MPa contained boehmite as the major phase. Similar effect of the supercritical water density on the dehydroxylation processes in γ-AlOOH as well as in $BaTiO_3$ were reviewed by Hayashi et al. [44].

Phase transformation of boehmite into α-alumina in a water medium under supercritical conditions has been extensively studied previously [32,42,45]. The observed evolution of the powders' morphology derived two separate viewpoints on the alumina formation and growth. On one hand, Suchanek [42] found no evident orientation of boehmite particles on the surfaces of alumina crystals to prove the solid-state nature of the alumina nucleation and growth and supposed dissolution-precipitation or surface diffusion processes to govern the reaction. Plyasunov [46] reported that the dissolved form of alumina in the supercritical water is $Al(OH)_3 \cdot H_2O$. On another hand, Ivakin et al. [32] revealed homogenous nucleation of α-Al_2O_3 in boehmite particles. Currently obtained ceramic samples contained phases different from $Al(OH)_3$, the presence of which might point to the dissolution-precipitation mechanism. However, the microstructure observed in the samples obtained at 380 °C and 350 MPa (Figure 6a) resembled that demonstrated by Yamaguchi et al. [7] for porous boehmite material CSPed from γ-$Al(OH)_3$ at milder conditions (250 °C, 270 MPa). The authors assumed that the large pores in the material were relics of the completely dissolved gibbsite particles, while the boehmite grains nucleated and grew from the solution separating them. Important to note that the pore space in boehmite could result from an intensive elimination of water during the gibbsite decomposition.

A study of the microstructural changes during the CSP at different temperatures and pressure values shows that dehydroxylation of the initial gibbsite on heating first results in the development of a fine-grained boehmite structure (Figure 7a). Further processing leads to a coalescence of these submicron grains and a formation of larger plate-like grains of boehmite (Figure 7b). Several authors [12,30] reported that at this stage of CSP, an interaction of the solid with the water medium leads to a dissociative adsorption of H_2O as well as to condensation of H^+ and OH^- with a formation of bridging oxygen between the metal ions. These processes have a decisive role in the oxygen ions diffusion, which facilitates and the mass transport between the grains and lowers the activation energy for the phase transitions. The boehmite grains of both rounded and plate-like morphologies under the CSP conditions tend to perform coalescence and finally transform homogenously into α-alumina modification (Figure 7c). Earlier, the coalescence of the particles was also demonstrated for the CSP of ZnO [47], $CaCO_3$ [3], and $Na_2Mo_2O_7$ [48].

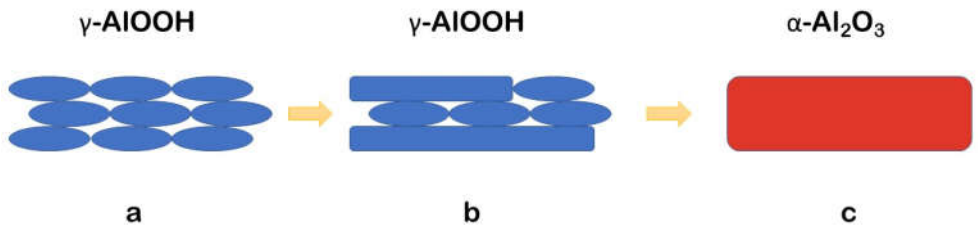

Figure 7. A schematic representation of the microstructural transformations during the CSP.

Regardless of the phase composition, the obtained ceramics possessed a relative density in a range of 58-65 %, which is close to the density of the conventionally pressed compacts. It is likely that the porosity of the samples containing boehmite was supported by water elimination accompanying the ongoing transformation into alumina. The shape of the formed α-Al_2O_3 grains appeared similar to that observed in its crystals synthesized from the boehmite powder in a medium of supercritical water [32,42]. Compared to the parent boehmite grains, the grains of α-alumina increased in the size

 doi:10.20944/preprints202405.0366.v1

and approached to their Wulffs shape [49], which indicates the fall of the driving force for the sintering and corresponds to the remaining porosity.

Interestingly, that α-Al_2O_3 ceramics currently produced by CSP demonstrated a porosity which is almost totally of the open type and was comparable to the recent results obtained by a traditional route [22,50–52]. This would make the obtained material highly attractive as a filter, thermal insulator, a component of polymer- and metal-ceramic composite, etc., when combined with sufficient mechanical strength and chemical resistivity. Energy- and time-saving CSP technique also would be a reason of competitiveness for these alumina ceramics compared to the related alumina materials conventionally sintered at a high temperature.

5. Conclusions

(1) For the first time, porous α-Al_2O_3 ceramics were processed directly by CSP at a temperature of 380-450 °C, a pressure of 220 MPa during 30 min. in a presence of pure water. The materials were characterized by predominately open-type porosity reaching 36 %.

(2) Under the studied CSP conditions, the initial γ-$Al(OH)_3$ powder undergoes dehydration leading to γ-AlOOH and possible minor χ-Al_2O_3 phases. Further processed, γ-AlOOH forms elongated grains, which coalesce into plate-like ones and transform into the grains of α-Al_2O_3.

(3) An increase in the applied pressure (up to 350 MPa) prevents the dehydration of γ-AlOOH and impedes the formation of the final α-Al_2O_3.

Author Contributions: Conceptualization, A.V.S. and Y.D.I.; methodology, A.A.K., M.V.K., and Y.D.I.; validation, M.V.K.; formal analysis, A.N.K. and L.A.A.; investigation, A.A.K., M.V.K., A.N.K., L.A.A., and Y.D.I.; resources, A.A.K., M.V.K., and Y.D.I.; data curation, A.A.K., M.V.K., A.N.K., L.A.A., and Y.D.I.; writing—original draft preparation, A.A.K.; writing—review and editing, A.A.K., A.V.S., and Y.D.I.; visualization, A.A.K.; supervision, A.V.S. and Y.D.I.; project administration, A.A.K.; funding acquisition, A.A.K. All authors have read and agreed to the published version of the manuscript.

Funding: This research was funded by the Russian Science Foundation, grant number 22-73-00318.

Institutional Review Board Statement: Not applicable.

Informed Consent Statement: Not applicable.

Data Availability Statement: The research data are available upon a request.

Acknowledgments: The authors would like to thank Tatiana V. Filippova from Chemistry Department of Lomonosov MSU for her kind help with XRD analysis. The study was supported in part by Lomonosov Moscow State University Program of Development.

Conflicts of Interest: The authors declare no conflicts of interest.

Appendix A

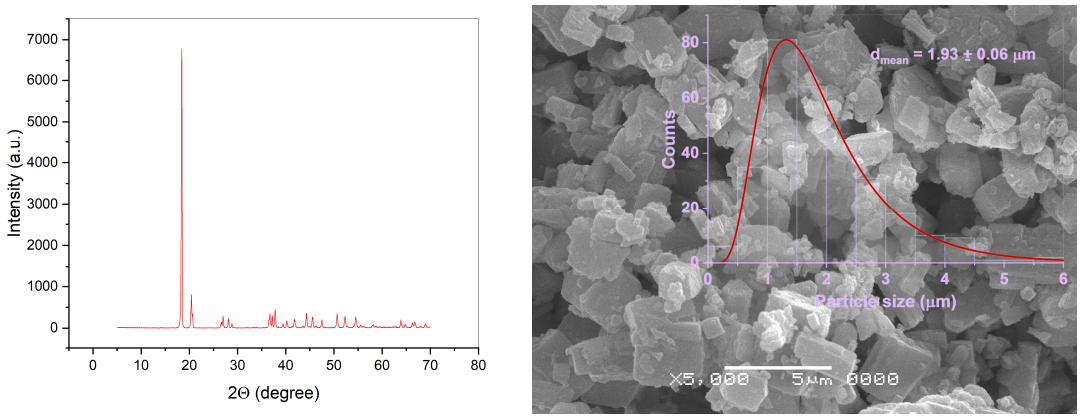

(**a**) (**b**)

Figure A1. XRD pattern (**a**) and SEM image (**b**) of the initial gibbsite (γ-$Al(OH)_3$) powder. The observed peaks correspond to PDF2 #000-076-1782. Size distribution is based on the measurements of 300 particles.

 doi:10.20944/preprints202405.0366.v1

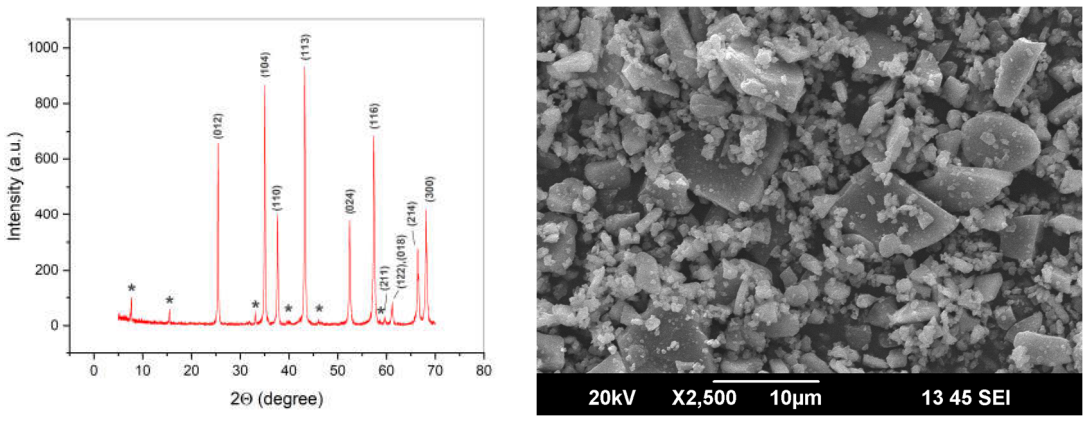

(**a**) (**b**)

Figure A2. XRD pattern (**a**) and SEM image (**b**) of a commercial α-Al_2O_3 additive to the initial γ-$Al(OH)_3$ powder. Miller indices correspond to α-Al_2O_3 phase (PDF2 #000-075-0782), asterisk indicates $Al_{22}O_{34}(H_2O)_2$ phase (PDF2 #000-070-1204). The calculated major phase content is 90.5 wt. %.

References

1. Randall, C.A.; Guo, J.; Baker, A.; Lanagan, M.T.; Guo, H. Cold Sintering Ceramics and Composites 2017.
2. Huang, Y.; Huang, K.; Zhou, S.; Lin, C.; Wu, X.; Gao, M.; Zhao, C.; Fang, C. Influence of Incongruent Dissolution-Precipitation on 8YSZ Ceramics during Cold Sintering Process. *Journal of the European Ceramic Society* **2022**, *42*, 2362–2369, doi:10.1016/j.jeurceramsoc.2021.12.072.
3. Zahabi, M.; Said, A.; Memari, A. Cold Sintering of Calcium Carbonate for Construction Material Applications. *ACS Omega* **2021**, *6*, 2576–2588, doi:10.1021/acsomega.0c04617.
4. Yamaguchi, K.; Hashimoto, S. Mechanism of Densification of Calcium Carbonate by Cold Sintering Process. *Journal of the European Ceramic Society* **2022**, *42*, 6048–6055, doi:10.1016/j.jeurceramsoc.2022.06.034.
5. Smirnov, A.V.; Ivakin, Yu.D.; Kornyushin, M.V.; Kholodkova, A.A.; Vasin, A.A.; Ayudinyan, S.; Kirakosyan, H.V. Effect of Activating Additives on the Cold Sintering Process of $(MnFeCoNiCu)_3O_4$ High-Entropy Ceramics. *Fine Chem. Technol.* **2022**, *17*, 439–449, doi:10.32362/2410-6593-2022-17-5-439-449.
6. Galotta, A.; Sglavo, V.M. The Cold Sintering Process: A Review on Processing Features, Densification Mechanisms and Perspectives. *Journal of the European Ceramic Society* **2021**, *41*, 1–17, doi:10.1016/j.jeurceramsoc.2021.09.024.
7. Yamaguchi, K.; Hashimoto, S. Effect of Phase Transformation in Cold Sintering of Aluminum Hydroxide. *Journal of the European Ceramic Society* **2024**, *44*, 2754–2761, doi:10.1016/j.jeurceramsoc.2023.12.054.
8. Thabet, K.; Quarez, E.; Joubert, O.; Le Gal La Salle, A. Application of the Cold Sintering Process to the Electrolyte Material $BaCe_{0.8}Zr_{0.1}Y_{0.1}O_{3-\delta}$. *Journal of the European Ceramic Society* **2020**, *40*, 3445–3452, doi:10.1016/j.jeurceramsoc.2020.03.043.
9. Guo, H.; Bayer, T.J.M.; Guo, J.; Baker, A.; Randall, C.A. Cold Sintering Process for 8 mol%Y_2O_3-Stabilized ZrO_2 Ceramics. *Journal of the European Ceramic Society* **2017**, *37*, 2303–2308, doi:10.1016/j.jeurceramsoc.2017.01.011.
10. Lai, Q.; Chen, J.; Chang, F.; Pei, J.; Liang, Y.; Chen, X.; Feng, Q.; Cen, Z.; Luo, N. Cold Sintering Process Assisted Sintering for 8YSZ Ceramic: A Way of Achieving High Density and Electrical Conductivity at a Reduced Sintering Temperature. *Ceramics International* **2023**, *49*, 14744–14749, doi:10.1016/j.ceramint.2023.01.070.
11. Grady, Z.; Ndayishimiye, A.; Randall, C. A Dramatic Reduction in the Sintering Temperature of the Refractory Sodium B″-Alumina Solid Electrolyte *via* Cold Sintering. *J. Mater. Chem. A* **2021**, *9*, 22002–22014, doi:10.1039/D1TA05933E.
12. Guo, N.; Liu, M.; Shen, J.-Y.; Shen, H.-Z.; Shen, P. Surface Hydrate-Assisted Low- and Medium-Temperature Sintering of MgO. *Scripta Materialia* **2022**, *206*, 114258, doi:10.1016/j.scriptamat.2021.114258.
13. Amrute, A.P.; Jeske, K.; Łodziana, Z.; Prieto, G.; Schüth, F. Hydrothermal Stability of High-Surface-Area α-Al_2O_3 and Its Use as a Support for Hydrothermally Stable Fischer–Tropsch Synthesis Catalysts. *Chem. Mater.* **2020**, *32*, 4369–4374, doi:10.1021/acs.chemmater.0c01587.
14. Huang, C.-L.; Wang, J.-J.; Huang, C.-Y. Sintering Behavior and Microwave Dielectric Properties of Nano Alpha-Alumina. *Materials Letters* **2005**, *59*, 3746–3749, doi:10.1016/j.matlet.2005.06.053.
15. Asimakopoulou, A.; Gkekas, I.; Kastrinaki, G.; Prigione, A.; Zaspalis, V.T.; Petrakis, S. Biocompatibility of α-Al_2O_3 Ceramic Substrates with Human Neural Precursor Cells. *JFB* **2020**, *11*, 65, doi:10.3390/jfb11030065.

16. Hashimoto, H.; Kojima, S.; Sasaki, T.; Asoh, H. α-Alumina Membrane Having a Hierarchical Structure of Straight Macropores and Mesopores inside the Pore Wall. *Journal of the European Ceramic Society* **2018**, *38*, 1836–1840, doi:10.1016/j.jeurceramsoc.2017.11.032.
17. Rytter, E.; Borg, Ø.; Enger, B.C.; Holmen, A. α-Alumina as Catalyst Support in Co Fischer-Tropsch Synthesis and the Effect of Added Water; Encompassing Transient Effects. *Journal of Catalysis* **2019**, *373*, 13–24, doi:10.1016/j.jcat.2019.03.013.
18. Liu, Y.; Ng, Z.; Khan, E.A.; Jeong, H.-K.; Ching, C.; Lai, Z. Synthesis of Continuous MOF-5 Membranes on Porous α-Alumina Substrates. *Microporous and Mesoporous Materials* **2009**, *118*, 296–301, doi:10.1016/j.micromeso.2008.08.054.
19. Dong, J.; Payzant, E.A.; Hu, M.Z.C.; Depaoli, D.W.; Lin, Y.S. Synthesis of MFI-Type Zeolite Membranes on Porous α-Alumina Supports by Wet Gel Crystallization in the Vapor Phase. *Journal of Materials Science* **2003**, *38*, 979–985, doi:10.1023/A:1022381326613.
20. Ohji, T.; Fukushima, M. Macro-Porous Ceramics: Processing and Properties. *International Materials Reviews* **2012**, *57*, 115–131, doi:10.1179/1743280411Y.0000000006.
21. Niu, L.; Qin, R.; Liu, Y.; Xin, J.; Wu, X.; Zhang, F.; Li, X.; Shao, C.; Li, X.; Liu, Y. Hierarchical Porous Alumina Ceramics as Multi-Functional Support with Excellent Performance. *Ceramics International* **2024**, *50*, 2611–2622, doi:10.1016/j.ceramint.2023.10.226.
22. Zhao, J.; Wang, L.; Mao, X.; An, L.; Liu, Y.; Wang, S.; Zhang, J.; Feng, K. Preparation and Properties of Porous Alumina Ceramics for Ultra-Precision Aerostatic Bearings. *Ceramics International* **2022**, *48*, 13311–13318, doi:10.1016/j.ceramint.2022.01.210.
23. Zhang, A.; Sang, K.; Zeng, D.; Liu, Q.; Guo, Y. Preparation and Properties of Porous Alumina with Inter-Locked Platelets Structure. *Ceramics International* **2022**, *48*, 25918–25922, doi:10.1016/j.ceramint.2022.05.268.
24. Dong, X.; Chua, B.W.; Li, T.; Zhai, W. Multi-Directional Freeze Casting of Porous Ceramics with Bone-Inspired Microstructure. *Materials & Design* **2022**, *224*, 111344, doi:10.1016/j.matdes.2022.111344.
25. Chen, H.; Pan, Y.; Chen, B.; Li, J.; Gui, Z.; Chen, J.; Yan, H.; Zeng, Y.; Chen, J. Fabrication of Porous Aluminum Ceramics beyond Device Resolution via Stereolithography 3D Printing. *Ceramics International* **2023**, *49*, 18463–18469, doi:10.1016/j.ceramint.2023.02.218.
26. Moshkovitz, M.Y.; Paz, D.; Magdassi, S. 3D Printing Transparent γ -Alumina Porous Structures Based on Photopolymerizable Sol–Gel Inks. *Adv Materials Technologies* **2023**, *8*, 2300123, doi:10.1002/admt.202300123.
27. Hérisson de Beauvoir, T.; Estournès, C. Translucent γ-AlOOH and γ-Al_2O_3 Glass-Ceramics Using the Cold Sintering Process. *Scripta Materialia* **2021**, *194*, 113650, doi:10.1016/j.scriptamat.2020.113650.
28. Kang, S.; Zhao, X.; Guo, J.; Liang, J.; Sun, J.; Yang, Y.; Yang, L.; Liao, R.; Randall, C.A. Thermal-Assisted Cold Sintering Study of Al_2O_3 Ceramics: Enabled with a Soluble γ-Al2O3 Intermediate Phase. *Journal of the European Ceramic Society* **2023**, *43*, 478–485, doi:10.1016/j.jeurceramsoc.2022.10.039.
29. Suleiman, B.; Zhang, H.; Ding, Y.; Li, Y. Microstructure and Mechanical Properties of Cold Sintered Porous Alumina Ceramics. *Ceramics International* **2022**, *48*, 13531–13540, doi:10.1016/j.ceramint.2022.01.232.
30. Gao, J.; Ding, Q.; Yan, P.; Liu, Y.; Hu, Y.; Ren, Y.; Wang, X.; Mustafa, T.; Fan, Y.; Jiang, W. Direct Cold Sintering of Translucent Gamma-Al_2O_3 Ceramics. *Journal of the European Ceramic Society* **2024**, *44*, 4225–4231, doi:10.1016/j.jeurceramsoc.2024.01.015.
31. Kholodkova, A.A.; Kornyushin, M.V.; Pakhomov, M.A.; Smirnov, A.V.; Ivakin, Y.D. Water-Assisted Cold Sintering of Alumina Ceramics in SPS Conditions. *Ceramics* **2023**, *6*, 1113–1128, doi:10.3390/ceramics6020066.
32. Ivakin, Yu.D.; Danchevskaya, M.N.; Muravieva, G.P. Induced Formation of Corundum Crystals in Supercritical Water Fluid. *Russ. J. Phys. Chem. B* **2015**, *9*, 1082–1094, doi:10.1134/S1990793115070088.
33. Yoshizawa, Y.; Hirao, K.; Kanzaki, S. Fabrication of Low Cost Fine-Grained Alumina Powders by Seeding for High Performance Sintered Bodies. *Journal of the European Ceramic Society* **2004**, *24*, 325–330, doi:10.1016/S0955-2219(03)00226-7.
34. Gates-Rector, S.; Blanton, T. The Powder Diffraction File: A Quality Materials Characterization Database. *Powder Diffr.* **2019**, *34*, 352–360, doi:10.1017/S0885715619000812.
35. Rodríguez-Carvajal, J. Recent Advances in Magnetic Structure Determination by Neutron Powder Diffraction. *Physica B: Condensed Matter* **1993**, *192*, 55–69, doi:10.1016/0921-4526(93)90108-I.
36. Vaitkus, A.; Merkys, A.; Sander, T.; Quirós, M.; Thiessen, P.A.; Bolton, E.E.; Gražulis, S. A Workflow for Deriving Chemical Entities from Crystallographic Data and Its Application to the Crystallography Open Database. *J Cheminform* **2023**, *15*, 123, doi:10.1186/s13321-023-00780-2.
37. Rietveld, H.M. A Profile Refinement Method for Nuclear and Magnetic Structures. *J Appl Crystallogr* **1969**, *2*, 65–71, doi:10.1107/S0021889869006558.
38. Schneider, C.A.; Rasband, W.S.; Eliceiri, K.W. NIH Image to ImageJ: 25 Years of Image Analysis. *Nat Methods* **2012**, *9*, 671–675, doi:10.1038/nmeth.2089.
39. MacKenzie, K.J.D.; Temuujin, J.; Okada, K. Thermal Decomposition of Mechanically Activated Gibbsite. *Thermochimica Acta* **1999**, *327*, 103–108, doi:10.1016/S0040-6031(98)00609-1.

40. Lamouri, S.; Hamidouche, M.; Bouaouadja, N.; Belhouchet, H.; Garnier, V.; Fantozzi, G.; Trelkat, J.F. Control of the γ-Alumina to α-Alumina Phase Transformation for an Optimized Alumina Densification. *Boletín de la Sociedad Española de Cerámica y Vidrio* **2017**, *56*, 47–54, doi:10.1016/j.bsecv.2016.10.001.
41. Chen, B.; Xu, X.; Chen, X.; Kong, L.; Chen, D. Transformation Behavior of Gibbsite to Boehmite by Steam-Assisted Synthesis. *Journal of Solid State Chemistry* **2018**, *265*, 237–243, doi:10.1016/j.jssc.2018.06.010.
42. Suchanek, W.L. Hydrothermal Synthesis of Alpha Alumina (α-Al_2O_3) Powders: Study of the Processing Variables and Growth Mechanisms. *Journal of the American Ceramic Society* **2010**, *93*, 399–412, doi:10.1111/j.1551-2916.2009.03399.x.
43. Ingram-Jones, V.J.; Slade, R.C.T.; Davies, T.W.; Southern, J.C.; Salvador, S. Dehydroxylation Sequences of Gibbsite and Boehmite: Study of Differences between Soak and Flash Calcination and of Particle-Size Effects. *J. Mater. Chem.* **1996**, *6*, 73, doi:10.1039/jm9960600073.
44. Hayashi, H.; Hakuta, Y. Hydrothermal Synthesis of Metal Oxide Nanoparticles in Supercritical Water. *Materials* **2010**, *3*, 3794–3817, doi:10.3390/ma3073794.
45. Ivakin, Yu.D.; Danchevskaya, M.N.; Muravieva, G.P. Recrystallization of Zinc Oxide in a Sub- and Supercritical Water Medium. *Russ. J. Phys. Chem. B* **2019**, *13*, 1189–1200, doi:10.1134/S199079311907011X.
46. Plyasunov, A.V. Predicting Solubility of Oxides of Metals and Metalloids in Supercritical Water. *Ind. Eng. Chem. Res.* **2020**, *59*, 970–980, doi:10.1021/acs.iecr.9b06542.
47. Smirnov, A.V.; Kornyushin, M.V.; Kholodkova, A.A.; Melnikov, S.A.; Stepanov, A.D.; Fesik, E.V.; Ivakin, Y.D. Cold Sintering Process of Zinc Oxide Ceramics: Powder Preparation and Sintering Conditions Effects on Final Microstructure. *Inorganics* **2022**, *10*, 197, doi:10.3390/inorganics10110197.
48. Ndayishimiye, A.; Fan, Z.; Mena-Garcia, J.; Anderson, J.M.; Randall, C.A. Coalescence in Cold Sintering: A Study on Sodium Molybdate. *Open Ceramics* **2022**, *11*, 100293, doi:10.1016/j.oceram.2022.100293.
49. Marmier, A.; Parker, S.C. *Ab Initio* Morphology and Surface Thermodynamics of $\alpha - Al_2O_3$ *Phys. Rev. B* **2004**, *69*, 115409, doi:10.1103/PhysRevB.69.115409.
50. Alzukaimi, J.; Jabrah, R. The Preparation and Characterization of Porous Alumina Ceramics Using an Eco-friendly Pore-forming Agent. *Int J Applied Ceramic Tech* **2019**, *16*, 820–831, doi:10.1111/ijac.13126.
51. Kerolli Mustafa, M.; Gabelica, I.; Mandić, V.; Veseli, R.; Ćurković, L. Reusing Waste Coffee Grounds in the Preparation of Porous Alumina Ceramics. *Sustainability* **2022**, *14*, 14244, doi:10.3390/su142114244.
52. Vemoori, R.; Bejugama, S.; Khanra, A.K. Fabrication and Characterization of Alumina and Zirconia-Toughened Alumina Porous Structures. *Ceramics International* **2023**, *49*, 21708–21715, doi:10.1016/j.ceramint.2023.03.310.